Local surface electronic response of Bi₂Te₃ topological insulator upon europium doping

Gilberto Rodrigues-Junior,[1] Thaís Chagas [ ],[2] Rafael Reis,[1] Paulo Victor Sciammarella,[3] Celso I. Fornari [ ],[4]
Paulo H. O. Rappl,[5] Eduardo Abramof,[5] Rogério Magalhães-Paniago,[1] and Ângelo Malachias [ ][1,*]

[1]*Departamento de Física, ICEx, Universidade Federal de Minas Gerais–UFMG, Avenida Antonio Carlos, 6627,
Belo Horizonte–MG, CEP 30123-970, Brazil*
[2]*Department Physik, Universität Siegen, Walter-Flex-Straße 3, 57072 Siegen, Germany*
[3]*Departamento de Física, Universidade Federal de Viçosa–UFV, Viçosa–MG, CEP 36570-000, Brazil*
[4]*Experimentelle Physik VII and Würzburg-Dresden Cluster of Excellence ct.qmat, Universität Würzburg,
Am Hubland, 97074 Würzburg, Germany*
[5]*Grupo de Pesquisa e Desenvolvimento em Materiais e Plasma, GPDMP, Instituto Nacional de Pesquisas Espaciais–INPE,
São José dos Campos–SP, CEP 12245-970, Brazil*

The most relevant characteristic of a topological insulator material is the presence of edge/surface states that are protected by the bulk topology, and therefore, insensitive to nonmagnetic disorder. However, if such disorder is induced by magnetic atoms or the topological insulator is subjected to an external magnetic field, the time-reversal symmetry is expected to break down, affecting the robustness of the edge/surface states. In this work, europium (Eu)-doped bismuth telluride thin films were grown by molecular beam epitaxy in order to analyze the effect of a small fraction of atoms with magnetic properties on topologically protected surface states. For films with different Eu concentrations, morphological and electronic characterizations were carried out using atomic force microscopy, scanning tunnelling microscopy, and scanning tunnelling spectroscopy (STS) techniques. The results show that, regardless of the Eu concentration, the layered structure characteristic of the Bi₂Te₃ phase is maintained. However, large (>2%) Eu concentrations induce the appearance of protrusions and clusters on the surface of the films. The STS measurements show the presence of surface states for pure and low-content Eu:Bi₂Te₃. The suppression of surface states is indicated by STS spectra in regions with well-defined gaps for some locally limited regions of our samples with large concentration of Eu atoms. From density functional theory we are able to show that the Eu substitutional impurity at the Bi site is not the main mechanism responsible for the observed changes in the topological insulator band structure. Furthermore, the magnetic properties of europium are not the key factor dictating the different Bi₂Te₃ local surface electronic properties experimentally observed by STS, which are mostly affected by alloying and atom replacement, which induce a chemical modification of the surface potential.

I. INTRODUCTION

Topological insulators (TIs) are among the most important recent discoveries in material physics. They have been the focus of intensive research by several theoretical and experimental groups in the last years, not only for their new and exotic physics but also for the considerable potential applications in spintronics devices and quantum computing [1–3]. These materials are characterized by having an energy gap separating the valence and conduction bands, but exhibiting gapless metallic states in their edges or surfaces, protected by time-reversal symmetry (TRS) [4]. Consequently, backscattering of the topological states by nonmagnetic disorders is completely suppressed [5–7].

Three-dimensional topological insulators were theoretically predicted [8–10] and later experimentally verified [11–13] for stoichiometric compounds of group V-VI chalcogenide semiconductors, which exhibit topological properties at room temperature. Bi₂Te₃, Bi₂Se₃, and Sb₂Te₃ have a simple band structure with a band gap of the order of a few hundred meV (up to 300 meV in Bi₂Se₃ and 170 meV in Bi₂Te₃) [14–17]. As in a typical semiconductor, the valence and conduction bands are associated with the *p* and *s* orbitals, respectively. Due to the strong spin-orbit coupling (SOC), the *p* orbital can be pulled up in energy above the *s* orbital resulting in a band inversion at the center of the Brillouin zone (Γ point). This property assigns a bulk nontrivial topological characteristic and, consequently, robust spin-polarized states with a linear dispersion are observed at the surface, forming a single Dirac cone.

The quantitative influence of magnetic dopants on materials with topological properties is still an open question. From the theoretical point of view, a magnetic impurity distributed in the crystalline lattice of a TI material acts as a locally applied magnetic field, breaking the TRS [18–20]. Consequently, Kramer's degeneracy at the Γ point is lifted giving rise to massive fermions subjected to backscattering processes.

An understanding of how magnetic impurities influence the topological surface states can provide a prototypical scenario that is useful for, e.g., future realization of the quantum anomalous Hall effect (QAHE) [21], topological magnetoelectric effects [22], and development of devices with well-defined spin channels [23]. In this sense, some efforts have been made aiming to test the robustness of surface states experimentally [24–27] and to investigate the manifestation of ferromagnetic properties [28–30]. These were already observed in Bi_2Te_3 and Bi_2Se_3 crystals doped with transition metal elements both in the bulk crystals [28] and epitaxial thin films [29]. However, a local investigation of the impact of magnetic dopants on the topological surface states considering not only long-range magnetic ordering effects is still scarce.

In this work, we studied the effect of europium (Eu) doping on Bi_2Te_3 thin films grown by molecular beam epitaxy. For films with different Eu concentrations, morphological and electronic characterizations were carried out using atomic force microscopy (AFM), scanning tunneling microscopy (STM), and scanning tunneling spectroscopy (STS) techniques. Raman spectroscopy measurements and density functional theory (DFT) calculations were also performed.

Since europium is a rare earth (RE) element with a large magnetic moment ($\sim 7.91\,\mu_B$) [31], its influence on Bi_2Te_3 topological surface states can be studied locally by STM/STS due to the surface-sensitive nature of the STM probe (STS measurements are sensitive to a 5–10 nm surface range surrounding the tip), differing from experiments that study large surface area effects such as angle-resolved photoemission spectroscopy (ARPES) [32].

II. METHODS

A. Growth

All bismuth telluride (Bi_2Te_3) thin films were grown by MBE on barium fluoride (BaF_2) substrates oriented along the (111) crystallographic direction, following the same procedure and growth parameters established in Refs. [32,33]. In summary, BaF_2 substrates were kept at a temperature of $270\,°C$ and the growth was established using three effusion cells. One cell was filled with nominal Bi_2Te_3, while two others contained elemental Te. These were used to keep the desired Bi:Te growth ratio. In order to achieve the desired doping concentration, a fourth cell charged with europium (Eu) was used. Bi_2Te_3:Eu growth conditions used here were carefully chosen to obtain high crystalline quality and stoichiometric bismuth telluride films with substitutional Eu atoms. In practice, the substrate temperature deposition window is narrow for epitaxial growth of this kind of material and Eu diffusion will be limited by this parameter. The parameters used here were found to lead to a low deposition rate and relatively low surface mobility, which reduce the chances of Eu clustering [32].

A series of samples with nominal Eu concentration ranging from 0% (pure Bi_2Te_3) to 11% and 50 nm Bi_2Te_3:Eu film thickness were grown. In order to protect the surface of these films from oxidation, an amorphous Te cap layer was deposited on Bi_2Te_3 after growth and subsequently removed in vacuum for STM/STS measurements. A complete description

of the surface protection of the Bi_2Te_3 films with amorphous Te layers can be found in Ref. [34].

B. Structural/electronic characterization

STM and STS measurements were performed under ultrahigh vacuum conditions in an Omicron-VT STM system operating at room temperature, with a base pressure of 1.0×10^{-10} mbar. All STM images were acquired in constant current mode and for STS measurements a lock-in amplifier (operating at 3000 Hz) was used to obtain differential conductance (dI/dV) curves directly. AFM measurements were carried out in a FlexAFM Nanosurf microscope, operating in tapping (semicontact) mode within an environment with controlled humidity, always kept below 30%.

Raman spectroscopy measurements were performed at room temperature using a Renishaw inVia confocal micro-Raman spectrometer operating in backscattering geometry. As the excitation source, a 632.8 nm HeNe laser line was used, and the laser power was carefully adjusted to 0.07 mW in order to avoid heating at the sample position. Focusing was provided by an optical microscope equipped with a $50\times$ and 0.75 NA objective lens, generating a laser spot diameter of around 1 μm at the sample.

C. Band structure simulation

In order to investigate the effects of europium incorporation on the band structure of bismuth telluride we carried out DFT calculations for different doping levels, as implemented in the QUANTUM ESPRESSO software package [35]. The calculations utilize the Perdew-Burke-Ernzerhof (PBE) generalized gradient approximation (GGA) of the exchange-correlation potential [36], with fully relativistic effects included in the pseudopotential to account for spin-orbit coupling effects. A plane-wave cutoff of 55 Ry was used for wave functions, and a 5 mRy smearing (using Marzari and Vanderbilt's scheme [37]) was employed to numerically smooth out the metallic occupation of the electronic states. For the surface calculations, a $15 \times 15 \times 1$ Monkhorst-Pack k-point mesh was used with a slab supercell geometry [38]. We studied the (111) Bi_2Te_3 surface using a slab method with five quintuple layers (QLs). Each QL consists of five atomic planes with Te^1-Bi-Te^2-Bi-Te^1 atomic order.

Theoretically, a europium atom can occupy any site within the QL, namely the Bi site or one of the two nonequivalent Te lattice sites, Te^1 and Te^2. However, recent studies based on formation energy calculations demonstrated a preference for europium atoms to occupy bismuth sites [39]. Based on this study, our DFT calculations were conducted with an Eu doping level obtained by randomly replacing Bi atoms with Eu atoms throughout the bismuth telluride QLs.

III. RESULTS

A. Morphological characterization

In order to analyze the europium incorporation in Bi_2Te_3 thin films a series of AFM and STM topographic images was measured. The left panels of Fig. 1 show large area ($>1\,\mu$m) AFM images for pure Bi_2Te_3 samples [Fig 1(a)] as well as
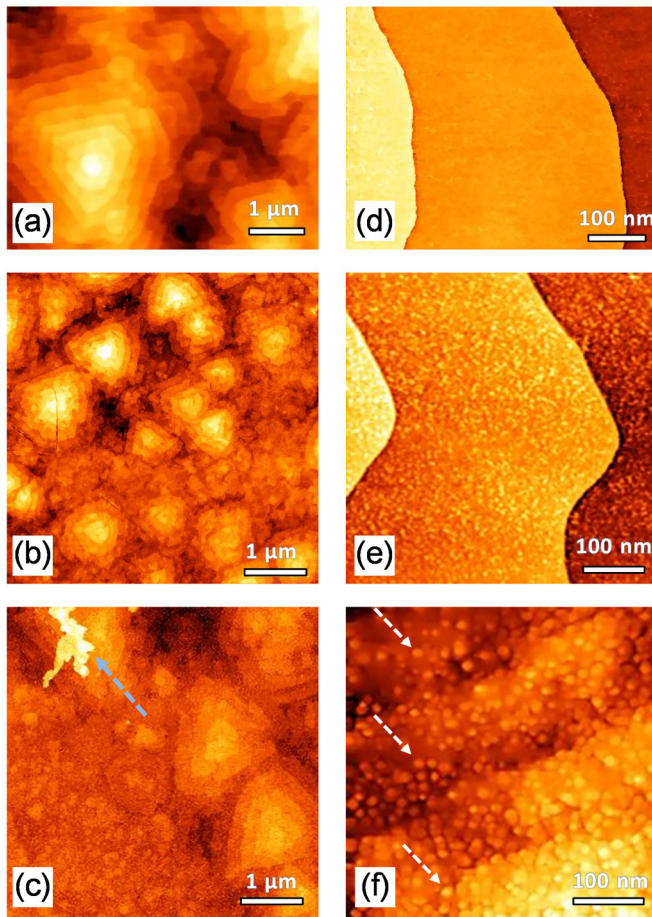
FIG. 1. (Left panels) Large scale AFM topographic images for Bi_2Te_3 samples with different Eu concentrations: (a) pure Bi_2Te_3, (b) 2% Eu-doped sample, and (c) 11% Eu-doped sample. (Right panels) Small scale STM topographic images on the surface of pure Bi_2Te_3 (d), 2% Eu-doped Bi_2Te_3 (e), and 11% Eu-doped Bi_2Te_3 (f). Dashed arrows highlight the segregation region (blue) and small protrusions (white) distributed along the QL terraces in the Eu-doped samples. STM images were acquired using $I = 400$ pA and $V = 1$ V.

FIG. 2. AFM topographic image showing protrusions or possible clusters associated with the europium deposition process distributed along the Bi_2Te_3 surface for the sample grown with 2% Eu (a,b) and for the sample grown with 11% Eu (c,d). An extreme case where the region is characterized by an all-covered surface is shown in (d). White dashed circles represent clusters, blue dashed arrow represents regions of segregation, and white dashed arrows represent small protrusions.

with different Eu concentrations [Figs. 1(b) and 1(c)]. As observed, the surface morphology of films grown with 2% Eu [Fig. 1(b)] and 11% Eu [Fig. 1(c)] presents spiral-shaped triangular pyramid domains with terraces of approximately one QL height (1 nm) that are characteristic of the Bi_2Te_3 undoped phase [Fig. 1(a)] [33]. However, in the sample with 11% Eu, it is possible to observe traces of segregation as spotlighted by the blue dashed arrow in Fig. 1(c) that may indicate an incomplete Eu incorporation in substitutional sites of the Bi_2Te_3 matrix.

A detailed view of these domains is provided by STM images presented in the right panels of Fig. 1. In these panels, the layered structure of pure Bi_2Te_3 [Fig. 1(d)] remains intact regardless of the presence of Eu in the films [as seen in Figs. 1(e) and 1(f) by the step edges]. In contrast, for films grown with 2% [Fig. 1(e)] and 11% Eu [Fig. 1(f)] small protrusions with typical height of 3–5 nm distributed along the QL terraces can be observed [see white dashed arrows in Fig. 1(f)]. This fact, associated with the segregation region, seen in the AFM
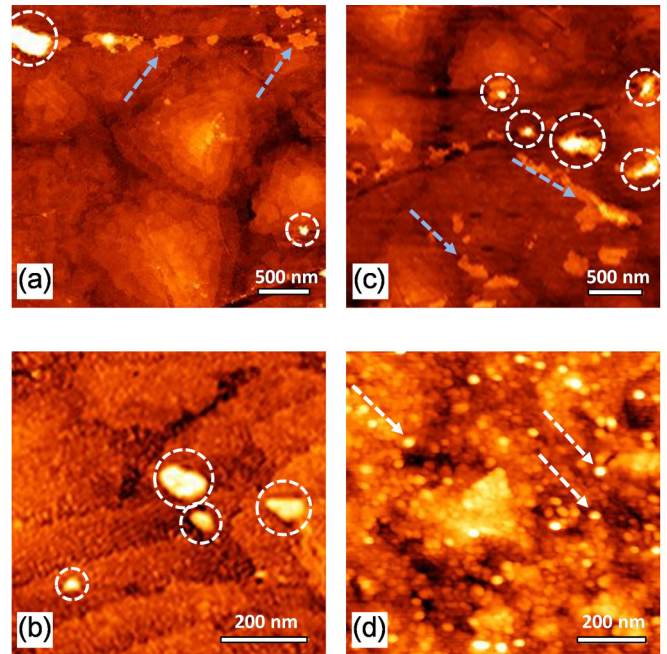
images for the sample with 11% Eu, indicates that during the epitaxial growth process, Eu atoms are not completely inserted into the Bi_2Te_3 crystal structure, forming clusters at the surface.

The presence of small protrusions or possible clusters, associated with the Eu deposition process, was investigated by performing several AFM measurements along different regions of the surface of the Eu-doped films. Some of these measurements are shown in Fig. 2, for 2% Eu-doped films (left panel) and for 11% Eu films (right panel). Differently from what was observed in previous studies where clusters start to appear at a threshold of Eu concentration above 4% [32], the AFM images represented in Fig. 2(a) indicate the presence of clusters (typical height of 10–16 nm) in the sample grown with 2% Eu; these features are highlighted by the white dashed circles. In this region of the sample surface, it is also possible to observe traces of segregation (see blue dashed arrows). A detailed view of the clusters that tend to nucleate on the terrace of the Bi_2Te_3 QL are observed in Fig. 2(b). In the sample with 11% Eu, the presence of clusters and regions of possible Eu segregation is more evident [Fig. 2(c)]. Furthermore, for this concentration of Eu, it is possible to find regions along the sample surface whose morphology changes drastically as shown in Fig. 2(d), where the pyramidal domains appear to be completely covered with Eu atoms or other crystalline phases such as EuTe. This is an indication of limited solubility of Eu atoms into the Bi_2Te_3 matrix during the epitaxial growth process.
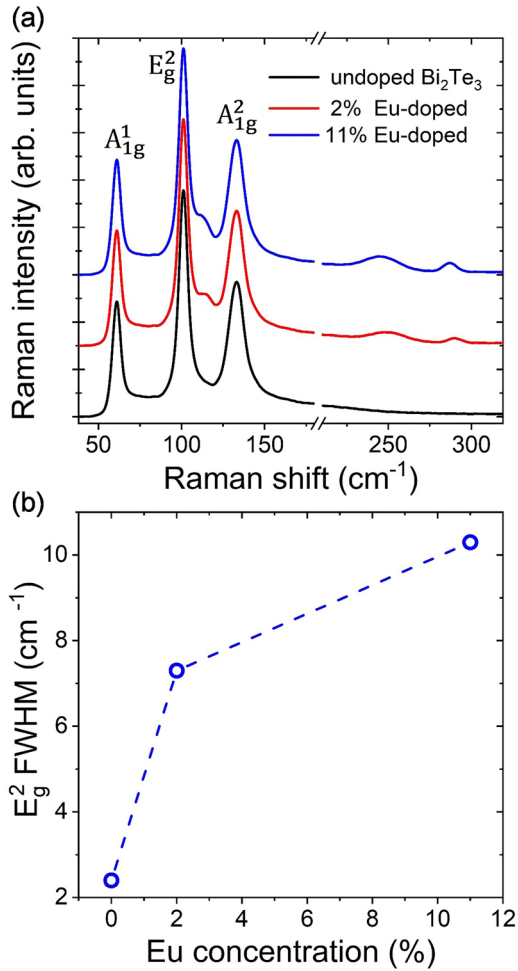
FIG. 3. (a) Bi_2Te_3 Raman spectra as a function of Eu concentration. In addition to the three characteristic peaks of the Bi_2Te_3 phase (A_{1g}^1, E_g^2, and A_{1g}^2), it is possible to observe three additional peaks in the doped samples that matched with the EuTe phase indicating the coexistence of a secondary phase for some regions of the doped samples. (b) The full width at half maximum (FWHM) of the E_g^2 mode as a function of Eu concentration.

B. Raman characterization

The possibility of the formation of other phases during the Eu doping process was investigated by Raman spectroscopy. As described in the Methods section, the excitation laser probes an area of $1 \times 1\,\mu m^2$ at the sample region, which makes it possible to study the areas where some clusters are present. Figure 3(a) shows the Raman spectra obtained for Bi_2Te_3 films grown with different Eu concentrations ranging from 0% (undoped sample) to 2% and 11%. In addition to the three expected phonon modes for the Bi_2Te_3 phase, A_{1g}^1, E_g^2, and A_{1g}^2 [40–42], for samples with 2% and 11% Eu there are additional peaks located at positions 112, 246, and 287 cm^{-1}.

These three additional peaks are close to positions expected for the EuTe phase [43,44], which indicates that the presence of Eu atoms on the surface of Bi_2Te_3 may favor the formation of a second phase where atomic planes of Eu and Te are stacked along the growth direction according to Ref. [32] or are forming clusters of cubic EuTe (rocksalt structure). Based

on this evidence and on previous x-ray diffraction studies, the clusters observed in the AFM images [white dashed circles in Fig. 2(b)] for the Eu-doped samples can be associated with the EuTe phase, and this secondary phase already forms in the low Eu concentration regime (2% Eu-doped samples).

Additionally, it is important to notice that some Raman spectra (depending on the sample region) show a broadening of the peak associated with the in-plane vibration mode E_g^2 as the concentration of Eu in the films increases, as evaluated in Fig. 3(b). This broadening, which is more evident for Bi_2Te_3 samples with 11% Eu, can be attributed to an increase in bulk disorder and stronger electron-phonon interactions which result in a reduction of phonon lifetime in the presence of magnetic impurities [42].

C. Electronic characterization

After analyzing the impact of Eu atoms on the morphology of bismuth telluride thin films, in this section, we will address the effects of the incorporation of Eu on the electronic properties of Bi_2Te_3. A series of STS measurements (single point and area spectroscopy) were performed at several regions on the surface of Bi_2Te_3 films, basically considering three regions: far from any cluster, in the vicinity of clusters, and at the top of the clusters. A measurement of the local density of states (LDOS) on the Bi_2Te_3 sample surface with different Eu concentrations provides important information on the topological surface states behavior.

The STS spectrum shown in Fig. 4(a) was measured in the undoped sample and is taken as a reference for the analysis of the spectra referring to the Eu-doped samples. In this spectrum, the curve inflection points named E_{BCB} and E_{BVB} (vertical gray dashed lines) determine the bottom of the bulk conduction band (BCB) and the top of the bulk valence band (BVB) [27], respectively. The bulk energy gap can be defined by the energy separation between E_{BCB} and E_{BVB}. The linear conductance region located in the bulk band gap indicates the presence of topological surface states and the effect of Eu doping on the Bi_2Te_3 surface states can be observed through the behavior of the Dirac point energy (E_D). However, unlike Bi_2Se_3 films, the Dirac energy for Bi_2Te_3 is not directly accessible in STS measurements [26,27,45]. This is associated with the fact that the Dirac point in the bismuth telluride electronic structure is buried in the valence band, as evidenced by ARPES measurements [32,34]. Therefore, the E_D value can be obtained through the extrapolation method [27,45], i.e., extending the linear part in STS (dI/dV) spectra to intercept the bias voltage axis, as represented by red dashed lines in Figs. 4(a)–4(c). In all STS curves the zero energy (bias voltage) marks the Fermi level (E_F).

STS curves in regions away from any detectable cluster are shown in Figs. 4(b) and 4(c) for samples with 2% and 11% Eu, respectively. Although in some of these regions small protrusions are observed (see white dashed arrow in left panels of Fig. 1), this is not enough to destroy the topological surface states since the linear conductance region is still visible in these curves, being comparable to the spectrum before the Eu deposition. However, the presence of small protrusions on the Bi_2Te_3 surface shifts the Dirac point to more negative energies ($E_D = -260\,meV$ for 2% Eu and $E_D = -398\,meV$
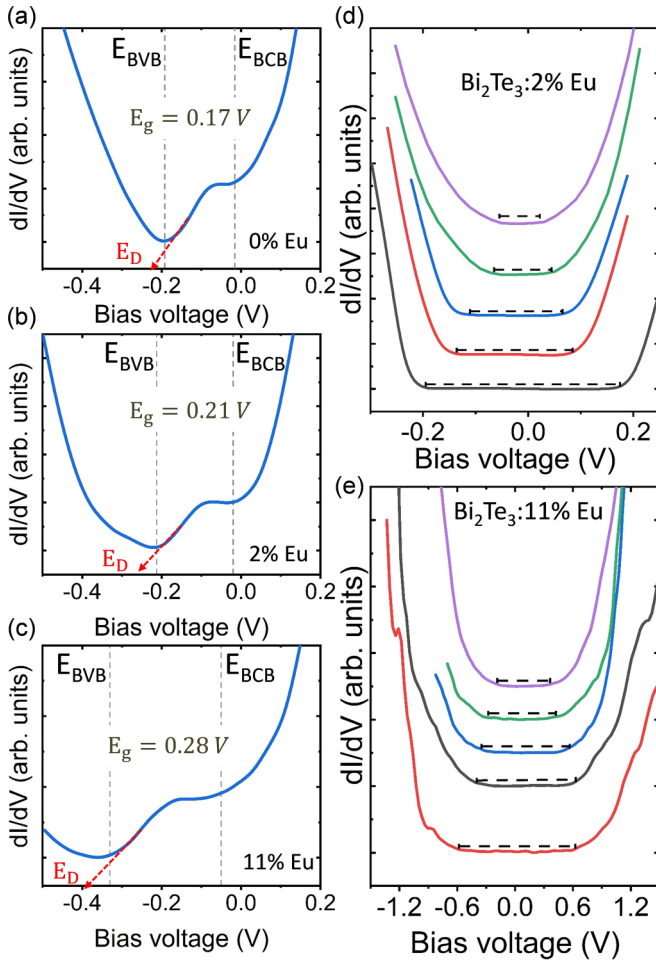
FIG. 4. (Left panels) A series of representative STS spectra taken at points along the sample surface where the signature of the surface states appears as a function of Eu concentrations. (a) Undoped Bi_2Te_3, (b) 2% Eu-doped, and (c) 11% Eu-doped. The Dirac point energy (E_D) is represented by the red dashed line and obtained by extrapolating the region of the curve in which the differential conductance (dI/dV) is linear. The edges of BVB and BCB determining the band gap are marked with vertical gray dashed lines. (Right panels) A series of representative STS spectra taken at points along the sample surface where the signature of the surface states disappears exhibiting a variable energy gap (region of zero differential conductance) for (d) 2% Eu-doped sample and (e) 11% Eu-doped sample. In all panels, the Fermi level is located at zero energy. It is important to note that the graphs are not represented with the x axis on the same scale and are displaced vertically with systematically increasing energy gap for better visualization.

for 11% Eu) when compared to the undoped sample value ($E_D = -215$ meV), indicating a possible n-type surface doping [indeed, the Fermi level (E_F) is situated near the BCB minimum]. In addition, the spectra are broader and a shift in the BCB minimum and BVB maximum is also observed, increasing the value of the bulk energy gap (E_g) in these regions; this effect is more evident for the sample with 11% Eu. The energy gap for Bi_2Te_3 was experimentally determined by resistivity measurements and the ARPES technique. Values of ~0.17 eV were retrieved [16,17].
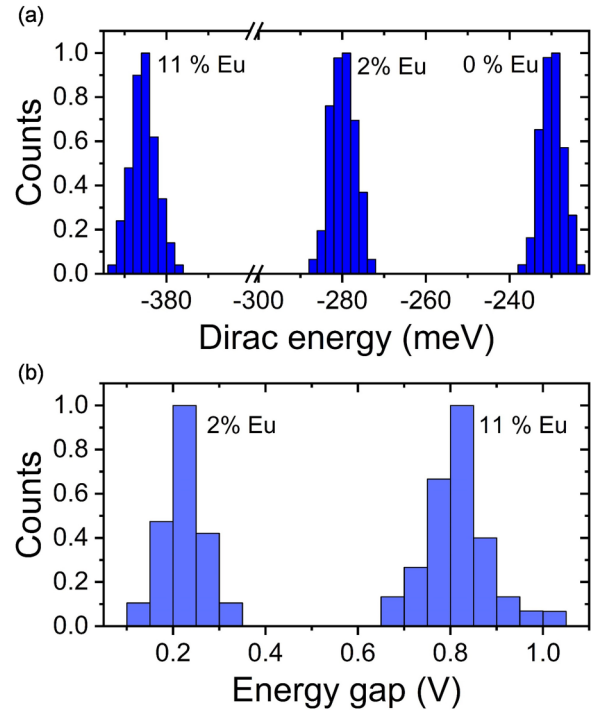

FIG. 5. (a) Histogram of Dirac energy (E_D) obtained from STS results on undoped (pristine) Bi_2Te_3, 2% Eu-doped sample and, 11% Eu-doped sample. (b) Histogram of energy gap (E_g) obtained from STS results on 2% Eu-doped sample and, 11% Eu-doped sample. A Gaussian function has been fitted to each histogram to quantify the mean Dirac energy value and mean energy gap value.

On the other hand, the STS spectra change severely when measurements are performed in regions with higher concentration of protrusions and clusters, as represented in Fig. 3. For samples with 2% Eu, the STS spectra [Fig. 4(d)] show a plateau region with zero conductance that resembles the STS expected for semiconductor materials. This suggests that there are regions along the Eu-doped Bi_2Te_3 surface where the signature of the surface states disappears. In addition, it is possible to observe a spatial fluctuation of energy gap values across the surface, represented by curves with different colors, shown with systematically increasing band gap for view clarity (see dashed horizontal lines), possibly associated with the nonuniform incorporation of Eu atoms in the Bi_2Te_3 matrix during the epitaxial growth that can induces defects in the surface. For samples with 11% Eu these features are more pronounced, exhibiting larger gap values, as shown in Fig. 4(e). Indeed, our STS measurements show that the energy gap values for both samples follow a Gaussian distribution with the center depending on the dopant concentration as shown in the statistical analysis presented in the Discussion section.

IV. DISCUSSION

The behavior of both the Dirac point and band gap observed in STS measurements for Bi_2Te_3 samples with different Eu concentrations can be quantified by analyzing the histograms shown in Figs. 5(a) and 5(b), respectively. The first set of histograms [Fig. 5(a)] was obtained from a

minimum of 100 STS curves for each sample, measured across regions of the sample surface without visible clusters, whereas the second set of histograms [Fig. 5(b)] was built from a minimum of 40 STS spectra for each sample with nonzero Eu concentration, measured in regions characterized by the presence of small protrusions and clusters. It is important to highlight that along the AFM/STM measurements these regions (clusters) are less common, showing that, regardless of the concentration of Eu, the doped films have a surface morphologically similar to the expected flat regions with 1 nm steps of pristine Bi_2Te_3 with the tetradymite quintuple layered structure, in consonance with Raman spectra shown in Fig. 3 and the x-ray diffraction and STEM results presented in Ref. [32].

In the histograms shown in Fig. 5(a), the Dirac point energy (E_D) was determined by extrapolating the linear region of the STS spectra that characterizes the existence of surface states as described in the previous section. Starting with the undoped sample (0% Eu), a set of STS measurements along the film surface resulted in an average Dirac point energy of $E_D = -(230 \pm 8)$ meV, which is in agreement with the values determined by ARPES measurements [34]. In contrast, the retrieved mean E_D values for different Eu concentrations are $E_D = -(280 \pm 10)$ meV for 2% Eu and $E_D = -(385 \pm 12)$ meV for 11% Eu, indicating that E_D shifts to more negative energies with respect to its Fermi level when Eu concentration increases.

Since STS is a surface-sensitive technique, this E_D displacement may be related to the increase in disorder and crystalline defects in the topmost QL associated with the doping process. It is important to mention that previous studies have shown that, regardless of the dopant concentration, the Eu atoms are preferentially inserted into the Bi_2Te_3 matrix in the divalent Eu^{2+} state [33]. Moreover, there is a tendency for Eu to occupy Bi sites at low Eu concentration regime (< 4% Eu) and to favor the formation of the EuTe phase at samples with higher Eu concentration (>4% Eu) [33]. Here we speculate that there is a competition between these two effects in the samples with 2% and 11% Eu.

The substitution of Bi atoms by Eu atoms is expected to induce acceptor behavior, since Eu atoms have lower valence (Eu^{2+} replaces Bi^{3+}), reducing the number of free electrons in the film [46]. This fact is not observed in our STS measurements. Indeed, the limited diffusion length of Eu atoms during the doping process and the onset of a secondary (EuTe) phase can introduce crystalline defects that act as electron donors, resulting in an *n*-type doping. The formation of the EuTe phase is more pronounced at the sample with 11% Eu, which is characterized by a larger occurrence of Te vacancies. Such effects may explain the shift of the Dirac point toward more negative bias than in the 2% Eu-doped sample, if one compares regions in both samples where the topological surface states appear.

Another important issue is observed through the spectra that indicate the existence of a gaplike structure in some regions of the Bi_2Te_3 samples doped with Eu. The histograms in Fig. 5(b) show that the sample with 2% Eu has an average energy gap value of $E_g = 0.22 \pm 0.05$ V while for the sample with 11% Eu this value increases to about $E_g = 0.8 \pm 0.2$ V; this behavior may indicate a local suppression of the topolog-

ical protection due to Eu doping. Indeed, for 2% Eu-doped Bi_2Te_3 films an energy gap of the order of 0.2 V is consistent with the expected gap value for the pure Bi_2Te_3 semiconductor material. Furthermore, the histogram indicates that in this sample the measured energy gap fluctuation is reduced around the mean value when compared to the values obtained in the sample with 11% Eu, suggesting that the substitutional incorporation of Eu atoms into the Bi_2Te_3 matrix is more effective in a low-concentration regime.

Considering the sample with 11% Eu, the high values of the energy gap found and the larger variation with respect to the mean value may indicate a possible local coexistence between the Bi_2Te_3, Eu_x ($Bi_{2-x}Te_3$), and EuTe phases due to the enhanced availability of Eu atoms on the surface and nonuniform incorporation into the Bi_2Te_3 crystalline structure. The energy gap values obtained in regions very close to the clusters can better elucidate this scenario.

Finally, Fig. 6(a) shows an STM image in a region very close to a cluster in the sample with 11% Eu. In the vicinity of the cluster, the film surface appears rough with no apparent step indicating poor crystalline quality. Furthermore, a series of STS spectra shows the behavior of LDOS as a function of the distance to the cluster. The STS measured at each colored dot is shown in Fig. 6(b) and allows one to observe a monotonic increase in the gap value as the distance to the cluster decreases. Over the cluster, a set of STS spectra (histogram shown in inset) shows an average energy gap value of approximately 2.0 ± 0.3 eV which is consistent with the expected value for EuTe crystals ($E_g \sim 2.4$ eV) [47]. This corroborates the fact that a second phase is formed during the epitaxial growth process, as also observed in the Raman measurements. Furthermore, the presence of such EuTe clusters on the surface modifies the Bi_2Te_3 electronic properties in such a way that the signature of the topologically protected surface states disappears in its vicinity.

The gap opening in the Dirac cone has already been observed in topological insulator samples doped with Fe, Mn, and Cr through ARPES and STS techniques [48–50]. Many of these works report sizable gaps (50–100 meV) with the increase of the magnetic impurities concentration. However, many other works indicate that even with a considerable concentration of magnetic atoms in the structure of the TI the Dirac cone remains preserved [51,52]. A striking feature is that high-quality Bi_2Te_3 thin films grown by MBE and doped with other RE elements exhibit different electronic properties. As can be seen in Refs. [53–55], Ho- and Gd-doped Bi_2Te_3 films investigated by ARPES confirmed the presence of an intact Dirac cone structure whereas Dy-doped films exhibit gapped topological surface states above a critical dopant concentration. In the case of Dy-doped Bi_2Te_3 films, the gap opening in the topological surface states was observed despite the absence of long-range magnetic order [55].

In order to elucidate the influence of Eu doping on the electronic structure of the bismuth telluride host crystal, *ab initio* calculations based on DFT were carried out as described in the Methods section. It is important to highlight that all calculations shown here were implemented without considering any antiferromagnetic and ferromagnetic ordering, i.e., taking into account only spin-orbit interactions. Such an approach makes possible the study of how the Bi_2Te_3 electronic
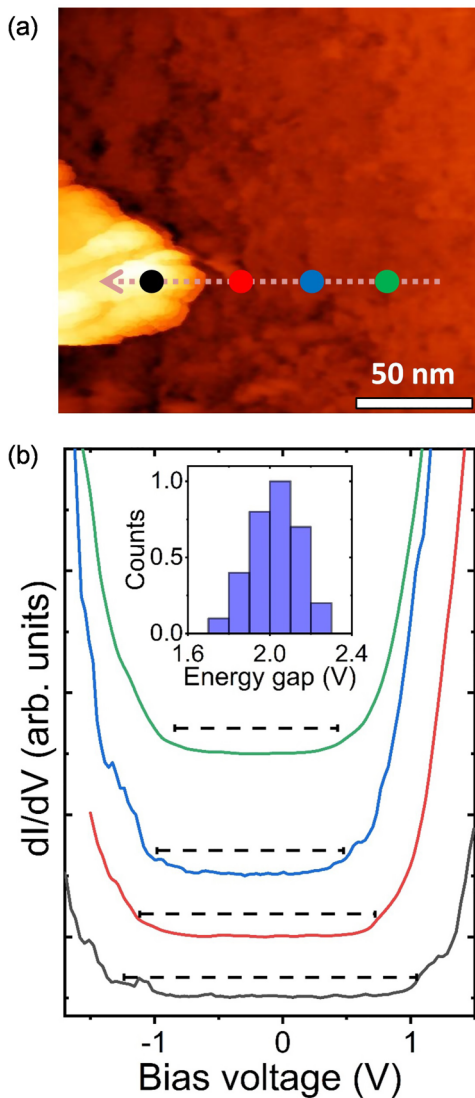
FIG. 6. (a) Detailed constant-current STM image in the vicinity of a cluster. Image acquired at $I = 500$ pA and $V = 1$ V. (b) LDOS as a function of cluster distance measured by STS at the points indicated by colored dots. The curves are offset vertically for clarity. Inset shows the histogram that accounts for the energy gap values over the cluster.

density of states and band structure, especially near the Dirac cone, change as Eu atoms are inserted into the crystalline structure. Such calculations can be used for comparison with the experimental results since all STS spectra shown in the previous paragraphs were measured at room temperature. A detailed DFT calculation taking into account the magnetic exchange coupling mechanism between Eu ions can be found in Ref. [31].

We start our discussion by considering the electronic structure of pristine bismuth telluride (undoped sample), shown in Fig. 7(a). The calculated band structure exhibits a Dirac cone–like structure (solid red line) at the Γ point (vertical black dashed line) connecting the bulk valence band and bulk conduction band, as expected for a three-dimensional topological insulator material [1–3]. The Dirac point energy (E_D)
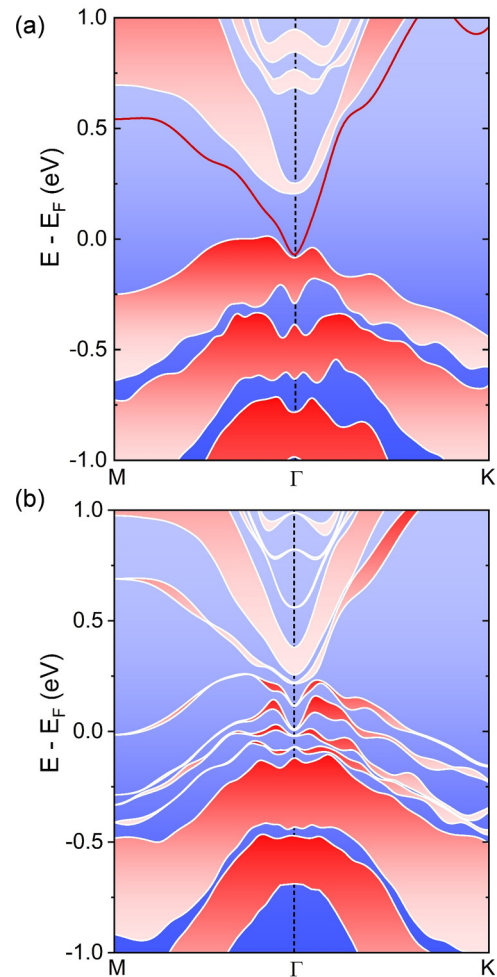

FIG. 7. Calculated band structure of (a) undoped Bi_2Te_3 and (b) 4% Eu-doped Bi_2Te_3 along the M-Γ-K directions of the surface Brillouin zone. Undoped Bi_2Te_3 band structure exhibits a Dirac cone (solid red line) connecting the valence and conduction bands (shaded red areas). On the other hand, the Dirac cone–like structure at the Γ point is lifted as well as the bands split due to the Eu incorporation process. Here the energy scale has been shifted so that the Fermi level lies at zero.

is buried into the valence band and situated $\sim$90 meV below the Fermi level (located at zero energy). In addition, the valence band maximum (VBM) and conduction band minimum (CBM) are localized at 0.02 and 0.20 eV, respectively. This position results in a band gap of $\sim$180 meV, which is in good agreement with theoretical and experimental values of Bi_2Te_3 crystal, even with the tendency of DFT to underestimate band gaps [8,16,17].

With respect to the Eu-doped Bi_2Te_3 samples, the impact of Eu impurities distributed along the crystalline lattice on the electronic structure can be seen in Fig. 7(b), where the band structure was calculated considering a nominal Eu concentration of 4%. One can observe that at this level of doping, the calculated band structure is clearly modified when compared to the undoped sample. Firstly, the Dirac cone structure at the Γ point (vertical black dashed line) is displaced toward higher energy values, accompanied by a significant band splitting that is more evident along the Γ-K direction. This behavior
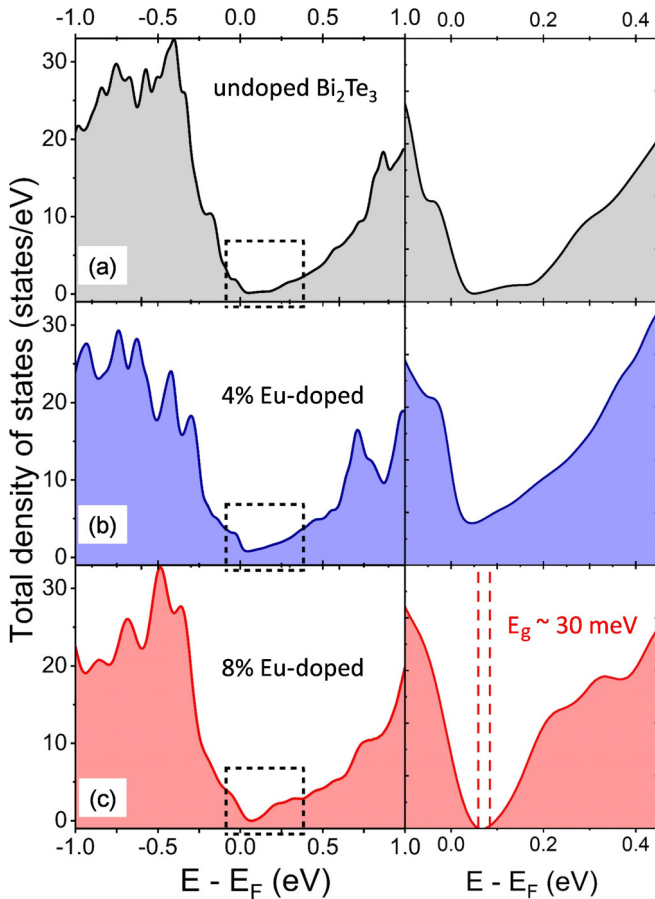
FIG. 8. (Left panels) DFT-based calculations of the total density of states (DOS) for Bi_2Te_3 doped with different Eu concentrations. (a) Undoped Bi_2Te_3, (b) 4% Eu-doped sample, and (c) 8% Eu-doped sample. In all panels, the Fermi level is located at zero energy. The right panels represent a close-up view in the vicinity of the Fermi level delimited by the dashed rectangle in the left panels. A gaplike structure is obtained by increasing the nominal Eu doping concentration to 8%.

is also observed in the bulk bands, especially for the branches close to the Fermi level. These effects, with tens of meV, could be measured only in a low-temperature ($\sim$4 K) ARPES setup, and cannot be evidenced by our STS measurements.

Additionally, along the M-Γ direction, an energy overlap region between the valence band and conduction band exists, which suggests a semimetal band structure. Indeed, at this doping level, the VBM and CBM are situated at 0.26 and 0.24 eV, respectively. Consequently, a pronounced upward shift of VBM with respect to the position of the undoped sample (about 0.24 eV) can be observed, whereas the CBM remains practically at the same position.

The changes in the electronic properties of Eu-doped Bi_2Te_3 become more evident when we analyze the total density of states. Figures 8(a) and 8(b) compare the calculated total density of states (DOS) for undoped Bi_2Te_3 and 4% Eu doped, respectively (left panels). It can be seen that, although new well-localized states appear in the form of clear peaks at -0.3 and 0.7 eV for the 4% Eu-doped sample, the main

difference occurs in the vicinity of the Fermi level, shown in detail in the right panels.

Comparing the right panels of Figs. 8(a) and 8(b), one observes that for 4% Eu-doped Bi_2Te_3 the range of the linearly dispersed states is not visible; indeed, this total DOS exhibits a V shape with a minimum around E_F characteristic of semimetal materials [56]. Interestingly, these results suggest that a 4% Eu-doping threshold is sufficient to modify the presence of topological surface states of Bi_2Te_3 even if no magnetic ordering is being considered. In our DFT calculations, a more abrupt change in the Bi_2Te_3 total DOS is obtained if the Eu doping concentration increases up to 8%, as shown in Fig. 8(c). At this doping level, the previously observed V-shape DoS for 4% Eu-doped is replaced by a U-shaped total DoS between 0 and 0.2 eV, which represents that a small gap $\sim$30 meV (vertical red dashed lines) opens at this energy range [right panel of Fig. 8(c)]. The occurrence of this sizable gap suggests that the topological nature of Bi_2Te_3 is sensitive to chemical effects and crystalline distortions introduced by the Eu-doping process even in the absence of magnetic ordering.

It is worth mentioning that the results obtained by DFT for Eu-doped bismuth telluride are not in full agreement with the STS spectra shown in Fig. 4, regardless of the dopant concentration. This fact suggests that the Eu incorporation process into the Bi_2Te_3 matrix during the epitaxial growth is not strictly substitutional at the Bi site even though this type of defect has the lowest formation energy [39]. Furthermore, the presence of EuTe clusters embedded in the Bi_2Te_3 volume or in the surface layer can influence the behavior of the surface states since the crystalline structure can suffer local distortions due to the difference in the lattice parameters of EuTe and Bi_2Te_3. Such features were not taken into account during DFT calculations.

Another important observation is that since our STS measurements were carried out at room temperature, the large gaps observed in Figs. 4(d) and 4(e) cannot be associated with ferromagnetic or antiferromagnetic ordering. Indeed, x-ray magnetic circular dichroism (XMCD) and magnetometry measurements show that Eu-doped Bi_2Te_3 thin films exhibit paramagnetic (PM) behavior at room temperature and a transition between the PM phase and antiferromagnetic phase only takes place for temperatures below 10 K [31]. Moreover, if the large magnetic moment of the Eu was the mechanism responsible for the measured gaps, the effect should be more evident for regions where Eu atoms are situated directly at the surface as illustrated in Figs. 1(e) and 1(f), which is not the simulated case. Recent theoretical works indicate a strong dependence of the topological surface states with the direction of the magnetization that appears due to the presence of magnetic atoms. First principles calculations in topological insulators doped with transition metals showed that an out of plane magnetization induces a gap opening in the Dirac cone, whereas an in-plane magnetization only displaces the Dirac cone [57]. In this sense, the occurrence of the gap together with evidence that surface states still exist in doped Bi_2Te_3 films may be attributed to the inhomogeneous Eu concentration on the surface, resulting in a spatially dependent magnetic field from the Eu atoms or surface clusters, as observed in Dy-doped films [55].

Another possibility is that the origin of the gaplike structure observed here is related to the fact that modifications in the topological states may only appear as a consequence of modifications in the structure of the bulk bands and are not dictated exclusively by the Eu magnetic properties. This fact can be corroborated taking into account that the gap opening observed in Mn-doped TI material is mediated by the presence of resonant Mn $3d$ states near the Dirac point [58]. However, as demonstrated in Ref. [32], Eu $3d \rightarrow 4f$ resonant photoemission experiments performed in Eu-doped Bi_2Te_3 samples indicate that the Eu $4f$ levels are located 1.7 eV below the Fermi level, presenting negligible spectral influence at this energy value.

Such kind of phase transition between a topological insulator and a trivial insulator has already been observed in nonmagnetic doped TI material [59]. In principle, it is possible that with the incorporation of a dopant, the bulk band structure reverts the band inversion, resulting in trivial insulator material [58,59]. Thus, the impurity scattering may play a more significant role than previously considered not solely due to its magnetic properties [27,59]. Indeed, the influence of Eu doping on Bi_2Te_3 bulk band structure can be evidenced from the displacement of the edges of the bulk conduction band and bulk valence band, as represented by vertical gray dashed lines in Figs. 4(a)–4(c), resulting in broader STS spectra as Eu content increases, in the surface regions where the signature of the surface states appears; i.e., the spectra where the linearly dispersed surface states are observed by the existence of a region within the bulk gap in which the differential conductance (dI/dV) is finite and varies linearly with bias voltage.

The fact that the gap opening in these samples [Fig. 4(d) and 4(e)] was not observed previously in ARPES measurements [32] may indicate that this feature is a local surface effect. Actually, the typical beam size in an ARPES system does not allow probing areas with a spatial resolution comparable to cluster/protrusion sizes, providing an average result (closer to pure Bi_2Te_3) while STM/STS results are able to probe purely local surface phenomena. One example of evidence of this is the fact that x-ray diffraction and scanning transmission electron microscopy (STEM) images on Eu-doped Bi_2Te_3 samples indicate films with good crystalline quality, suggesting that atomically disordered regions are less frequent [32]. Further experimental studies using low-temperature STS measurements may pro-

vide a concise scenario to understand the existence of the topological phase and band gap opening in the Eu-doped samples.

V. CONCLUSION

In this work, we studied the effect of the incorporation of Eu atoms in Bi_2Te_3 films grown by the MBE technique. A set of samples with different Eu concentrations was grown (pure Bi_2Te_3, and 2% and 11% Eu-doped Bi_2Te_3) and shows different morphological and electronic characteristics.

AFM and STM measurements show that, regardless of the Eu concentration in the films, the samples presented topography similar to that expected for pristine Bi_2Te_3 with pyramidal triangular domains distributed along the substrate surface. However, some AFM/STM measurements also indicate the presence of cluster-type defects which is more evident as Eu content in Bi_2Te_3 films increases. Furthermore, Raman spectroscopy measurements indicate an increase in disorders in the films as well as the formation of the EuTe phase for both Eu concentrations (2% and 11%).

Since previously low-temperature ($\sim$20 K) ARPES measurements were not able to study the magnetic ordering effect in Eu-doped Bi_2Te_3 films (antiferromagnetic onset temperature $\sim$10 K), the Dirac cone remains intact indicating that surface states exist even in the presence of magnetic impurities. Contrarily, our room-temperature STS measurements point out that considerable gaps appear already in the low Eu concentration regime which is not associated with long-range magnetic order. This fact indicates that along the sample surface, there are regions in which the presence of dopant disorders acts locally on the surface states.

According to our DFT calculations, doping with Eu systematically modifies the Bi_2Te_3 band structure. However, a Eu atom replacing a Bi atom is not the main mechanism responsible for the different characteristics observed in the Bi_2Te_3 local density of states measured by STS spectra.

[1] J. E. Moore, The birth of topological insulators, Nature (London) **464**, 194 (2010).

[2] W. Zhang, R. Yu, H.-J. Zhang, X. Dai, and Z. Fang, First-principles studies of the three-dimensional strong topological insulators Bi_2Te_3, Bi_2Se_3 and Sb_2Te_3, New J. Phys. **12**, 065013 (2010).

[3] D. Hsieh, Y. Xia, D. Qian, L. Wray, J. H. Dil, F. Meier, J. Osterwalder, L. Patthey, J. G. Checkelsky, N. P. Ong *et al.*, A tunable topological insulator in the spin helical Dirac transport regime, Nature (London) **460**, 1101 (2009).

[4] M. Hasan and C. Kane, Colloquium: Topological insulators, Rev. Mod. Phys. **82**, 3045 (2010).

[5] T. Fukui, T. Fujiwara, and Y. Hatsugai, Topological meaning of

Z_2 numbers in time reversal invariant systems, J. Phys. Soc. Jpn. **77**, 123705 (2008).

[6] R. Resta and D. Vanderbilt, Theory of polarization: A modern approach, in *Physics of Ferroelectrics*, edited by K. M. Rabe, C. H. Ahn, and J.-M. Triscone (Springer, Berlin, 2007), pp. 31–68.

[7] J. E. Moore and L. Balents, Topological invariants of time-reversal-invariant band structures, Phys. Rev. B **75**, 121306(R) (2007).

[8] H. Zhang, C.-X. Liu, X.-L. Qi, X. Dai, Z. Fang, and S.-C. Zhag, Topological insulators in Bi_2Se_3, Bi_2Te_3 and Sb_2Te_3 with a single Dirac cone on the surface, Nat. Phys. **5**, 438 (2009).

[9] L. Fu, C. L. Kane, and E. J. Mele, Topological Insulators in Three Dimensions, Phys. Rev. Lett. **98**, 106803 (2007).

[10] R. Roy, Topological phases and the quantum spin Hall effect in three dimensions, Phys. Rev. B **79**, 195322 (2009).

[11] Y. L. Chen, J. G. Analytis, J. -H. Chu, Z. K. Liu, S.-K. Mo, X. L. Qi, H. J. Zhang, D. H. Lu, X. Dai, Z. Zhang *et al.*, Experimental realization of a three-dimensional topological insulator, Bi_2Te_3, Science **325**, 178 (2009).

[12] Y. Xia, D. Qian, D. Hsieh, L. Wray, A. Pal, H. Lin, A. Bansil, Y. S. Hor D.Grauer, R. J. Cava, and M. Z. Hasan, Observation of a large-gap topological-insulator class with a single Dirac cone on the surface, Nat. Phys. **5**, 398 (2009).

[13] D. Hsieh, Y. Xia, D. Qian, L. Wray, F. Meier, J. H. Dil, J. Osterwalder, L. Patthey, A. V. Fedorov, H. Lin *et al.*, Observation of Time-Reversal-Protected Single-Dirac-Cone Topological-Insulator States in Bi_2Te_3 and Sb_2Te_3, Phys. Rev. Lett. **103**, 146401 (2009).

[14] J. Black, E. M. Conwell, L. Seigle, and C. W. Spencer, Electrical and optical properties of some $M_2^{V-B}N_3^{VI-b}$ semiconductors, J. Phys. Chem. Solids **2**, 240 (1957).

[15] E. Mooser and W. B. Pearson, New semiconducting compounds, Phys. Rev. **101**, 492 (1956).

[16] I. G. Austin, The optical properties of bismuth telluride, Proc. Phys. Soc. **72**, 545 (1958).

[17] C. -Y. Li, A. L. Ruoff, and C. W. Spencer, Effect of pressure on the energy gap of Bi_2Te_3, J. Appl. Phys. **32**, 1733 (1961).

[18] X.-L. Qi, T. L. Hughes, and S.-C. Zhang, Fractional charge and quantized current in the quantum spin Hall state, Nat. Phys. **4**, 273 (2008).

[19] X. -L. Qi, T. L. Hughes, and S.-C. Zhang, Topological field theory of time-reversal invariant insulators, Phys. Rev. B **78**, 195424 (2008).

[20] Q. Liu, C.-X. Liu, C. Xu, X.-L. Qi, and S.-C. Zhang, Magnetic Impurities on the Surface of a Topological Insulator, Phys. Rev. Lett. **102**, 156603 (2009).

[21] Y. Rui, W. Zhang, H.-J. Zhang, S.-C. Zhang, X. Dai, and Z. Fang, Quantized anomalous Hall effect in magnetic topological insulators, Science **329**, 61 (2010).

[22] Y. Tokura, K. Yasuda, and A. Tsukazaki, Magnetic topological insulators, Nat. Rev. Phys. **1**, 126 (2019).

[23] X. Kou, Y. Fan, M. Lang, P. Upadhyaya, and K.-L. Wang, Magnetic topological insulators and quantum anomalous hall effect, Solid State Commun. **215**, 34 (2015).

[24] L. A. Wray, S.-Y. Xu, Y. Xia, D. Hsieh, A. V. Fedorov, Y. S. Hor, R. J. Cava, A. Bansil, H. Lin, and M. Z. Hasan, A topological insulator surface under strong Coulomb, magnetic and disorder perturbations, Nat. Phys. **7**, 32 (2010).

[25] Y. L. Chen, J.-H. Chu, J. G. Analytis, Z. K. Liu, K. Igarashi, H.-H. Kuo, L. Qi, S. K. Mo, R. G. Moore, D. H. Lu *et al.*, Massive Dirac fermion on the surface of a magnetically doped topological insulator, Science **329**, 659 (2010).

[26] Y.-L. Wang, Y. Xu, Y.-P. Jiang, J.-W. Liu, C.-Z. Chang, M. Chen, Z. Li, C.-L. Song, L.-L. Wang, K. He *et al.*, Structural defects and electronic properties of the Cu-doped topological insulator Bi_2Te_3, Phys. Rev. B **84**, 075335 (2011).

[27] H. Beidenkopf, P. Roushan, J. Seo, L. Gorman, I. Drozdov, Y. S. Hor, R. J. Cava, and A. Yazdani, Spatial fluctuations of helical Dirac fermions on the surface of topological insulators, Nat. Phys **7**, 939 (2011).

[28] Y. S. Hor, P. Roushan, H. Beidenkopf, J. Seo, D. Qu, J. G. Checkelsky, L. A. Wray, D. Hsieh, Y. Xia, S.-Y. Xu *et al.*, Development of ferromagnetism in the doped topological insulator, Phys. Rev. B **81**, 195203 (2010).

[29] P. P. J. Haazen, J.-B. Laloë, T. J. Nummy, H. J. M. Swagten, P. Jarillo-Herrero, D. Heiman, and J. S. Moodera, Ferromagnetism in thin-film Cr-doped topological insulator Bi_2Se_3, Appl. Phys. Lett. **100**, 082404 (2012).

[30] Z. H. Zhou, Y.-J. Chien, and C. Uher, Thin-film ferromagnetic semiconductors based on $Sb_{2-x}V_xTe_3$ with T_C of 177 K, Appl. Phys. Lett. **87**, 112503 (2005).

[31] A. Tcakaev, V. B. Zabolotnyy, C. I. Fornari, P. Rüßmann, T. R. F. Peixoto, F. Stier, M. Dettbarn, P. Kagerer, E. Weschke, E. Schierle *et al.*, Incipient antiferromagnetism in the Eu-doped topological insulator Bi_2Te_3, Phys. Rev. B **102**, 184401 (2020).

[32] C. I. Fornari, H. Bentmann, S. L. Morelhao, T. R. F. Peixoto, P. H. O. Rappl, A.-V. Tcakaev, V. Zabolotnyy, M. Kamp, T.-L. Lee, C.-H. Min *et al.*, Incorporation of europium in Bi_2Te_3 topological insulator epitaxial films, J. Phys. Chem. C **124**, 16048 (2020).

[33] C. I. Fornari, P. H. O. Rappl, S. L. Morelhão, and E. Abramof, Structural properties of Bi_2Te_3 topological insulator thin films grown by molecular beam epitaxy on (111) BaF_2 substrates, J. Appl. Phys. **119**, 165303 (2016).

[34] C. I. Fornari, P. H. O. Rappl, S. L. Morelhão, T. R. F. Peixoto, H. Bentmann, F. Reinert, and E. Abramof, Preservation of pristine Bi_2Te_3 thin film topological insulator surface after *ex situ* mechanical removal of Te capping layer, APL Mater. **4**, 106107 (2016).

[35] P. Giannozzi, O. Baseggio, P. Bonfà, D. Brunato, R. Car, I. Carnimeo, C. Cavazzoni, S. de Gironcoli, P. Delugas, F. F.Ruffino, A. Ferretti, N. Marzari, I. Timrov, A. Urru, and S. Baroni, QUANTUM ESPRESSO toward the exascale, J. Chem. Phys. **152**, 154105 (2020).

[36] J. P. Perdew, K. Burke, and Y. Wang, Generalized gradient approximation for the exchange-correlation hole of a many-electron system, Phys. Rev. B **54**, 16533 (1996).

[37] N. Marzari, D. Vanderbilt, A. De Vita, and M. C. Payne, Thermal Contraction and Disordering of the Al(110) Surface, Phys. Rev. Lett. **82**, 3296 (1999).

[38] M. L. Cohen, M. Schlüter, J. R. Chelikowsky, and S. G. Louie, Self-consistent pseudopotential method for localized configurations: Molecules, Phys. Rev. B **12**, 5575 (1975).

[39] A. Baranovskiy, M. Harush, and Y. Amouyal, On the influence of rare earth dopants on thermal transport in thermoelectric Bi_2Te_3 compounds: An *ab initio* perspective, Adv. Theory Simul. **2**, 1800162 (2019).

[40] G. Rodrigues-Junior, L. A. B. Marçal, G. A. S. Ribeiro, P. H. Rappl, E. Abramof, P. V. Sciammarella, L. M. Guimarães, C. A. Pérez, and A. Malachias, Direct observation of large strain through van der Waals gaps on epitaxial Bi_2Te_3/graphite: Pseudomorphic relaxation and the role of Bi_2 layers on the Bi_xTe_y topological insulator series, Phys. Rev. Mater. **4**, 023602 (2020).

[41] O. Caha, A. Dubroka, J. Humlíček, V. Holý, H. Steiner, M. Ul-Hassan, J. Sánchez-Barriga, O. Rader, T. N. Stanislavchuk, A. A. Sirenko *et al.*, Growth, Structure, and electronic properties of epitaxial bismuth telluride topological insulator films on BaF_2 (111) substrates, Cryst. Growth Des. **13**, 3365 (2013).

[42] J. Zhang, Z. Peng, A. Soni, Y. Zhao, Y. Xiong, B. Peng, J. Wang, M. S. Dresselhaus, and Q. Xiong, Raman spectroscopy of

few-quintuple layer topological insulator Bi_2Se_3 nanoplatelets, Nano Lett. **11**, 2407 (2011).

[43] Y. Ousaka, O. Sakai, and M. Tachiki, Theory of Raman scattering in magnetically ordered phases of EuSe and EuTe, Solid State Commun. **23**, 589 (1977).

[44] G. Güntherodt and R. Zeyher, Spin-dependent Raman scattering in magnetic semiconductors, in *Light Scattering in Solids IV*, edited by M. Cardona and G. Güntherodt (Springer, Berlin, 1984) pp. 203–242.

[45] C. Parra, T. H. R. Cunha, A. W. Contryman, D. Kong, F. Montero-Silva, P. H. R. Gonçalves, D. D. dos Reis, P. Giraldo-Gallo, R. Segura, F. Olivares *et al.*, Phase separation of Dirac electrons in topological insulators at the spatial limit, Nano Lett. **17**, 97 (2017).

[46] N. A. Abdullayev, K. M. Jafarli, K. V. Aliguyeva, L. N. Aliyeva, S. S. Kahramanov, and S. A. Nemov, Effect of doping with rare-earth elements (Eu, Tb, Dy) on the conductivity of Bi_2Te_3 layered single crystals, Semiconductors **51**, 942 (2017).

[47] A. Mauger and C. Godart, The magnetic, optical, and transport properties of representatives of a class of magnetic semiconductors: The europium chalcogenides, Phys. Rep. **141**, 51 (1986).

[48] J. Kim, and S. H. Jhi, Magnetic phase transition in Fe-doped topological insulator Bi_2Se_3, Phys. Rev. B **92**, 104405 (2015).

[49] S. Kamboj, S. Das, A. Sirohi, R. R. Chowdhury, S. Gayen, V. K. Maurya, S. Patnaik, and G. Sheet, Suppression of transport spin-polarization of surface states with emergence of ferromagnetism in Mn-doped Bi_2Se_3, J. Phys.: Condens. Matter **30**, 355001 (2018).

[50] X. F. Kou, W. J. Jiang, M. R. Lang, F. X. Xiu, L. He, Y. Wang, Y. Wang, X. X. Yu, A. V. Fedorov, P. Zhang, and K. L. Wang, Magnetically doped semiconducting topological insulators, J. Appl. Phys. **112**, 063912 (2012).

[51] M. R. Scholz, J. Sánchez-Barriga, D. Marchenko, A. Varykhalov, A. Volykhov, L. V. Yashina, and O. Rader, Tolerance of Topological Surface States towards Magnetic Moments: Fe on Bi_2Se_3, Phys. Rev. Lett. **108**, 256810 (2012).

[52] D. Zhang, A. Richardella, D. W. Rench, S.-Y. Xu, A. Kandala, T. C. Flanagan, H. Beidenkopf, A. L. Yeats, B. B. Buckley, P. V. Klimov *et al.*, Interplay between ferromagnetism, surface states, and quantum corrections in a magnetically doped topological insulator, Phys. Rev. B **86**, 205127 (2012).

[53] S. E. Harrison, L. J. Collins-McIntyre, S.-L. Zhang, A. A. Baker, A. I. Figueroa, A. J. Kellock, A. Pushp, S. S. P. Parkin, J. S. Harris, and G. van der Laan, Study of Dy-doped Bi_2Te_3: Thin film growth and magnetic properties, J. Phys.: Condens. Matter **27**, 245602 (2015).

[54] S. Li, S. E. Harrison, Y. Huo, A. Pushp, H. T. Yuan, B. Zhou, A. J. Kellock, S. S. P. Parkin, Y.-L. Chen, T. Hesjedal, and J. S. Harris, Magnetic properties of gadolinium substituted Bi_2Te_3 thin films, Appl. Phys. Lett. **102**, 242412 (2013).

[55] S. E. Harrison, L. J. Collins-McIntyre, P. Schönherr, A. Vailionis, V. Srot, P. A. van Aken, A. J. Kellock, A. Pushp, S. S. P. Parkin, J. S. Harris *et al.*, Massive Dirac fermion observed in lanthanide-doped topological insulator thin films, Sci. Rep **5**, 15767 (2015).

[56] C. Zhao, M. Hu, J. Qin, B. Xia, C. Liu, S. Wang, D. Guan, Y. Li, H. Zheng, J. Liu, and J. Jia, Strain Tunable Semimetal-Topological-Insulator Transition in Monolayer 1T′-WTe_2, Phys. Rev. Lett. **125**, 046801 (2020).

[57] J. Henk, M. Flieger, I. V. Maznichenko, I. Mertig, A. Ernst, S. V. Eremeev, and E. V. Chulkov, Topological Character and Magnetism of the Dirac State in Mn-Doped Bi_2Te_3, Phys. Rev. Lett. **109**, 076801 (2012).

[58] J. Sánchez-Barriga, A. Varykhalov, G. Springholz, H. Steiner, R. Kirchschlager, G. Bauer, O. Caha, E. Schierle, E. Weschke, A. A. Ünal *et al.*, Nonmagnetic band gap at the Dirac point of the magnetic topological insulator $(Bi_{1-x}Mn_x)_2Se_3$, Nat. Commun. **7**, 10559 (2016).

[59] M. Brahlek, N. Bansal, N. Koirala, S.-Y. Xu, M. Neupane, C. Liu, M. Z. Hasan, and S. Oh, Topological-Metal to Band-Insulator Transition in Thin Films, Phys. Rev. Lett. **109**, 186403 (2012).